

THE SLOAN LENS ACS SURVEY. VI: DISCOVERY AND ANALYSIS OF A DOUBLE EINSTEIN RING[†].RAPHAËL GAVAZZI¹, TOMMASO TREU^{1,2,3}, LÉON V. E. KOOPMANS⁴, ADAM S. BOLTON^{5,6}, LEONIDAS A. MOUSTAKAS⁷,
SCOTT BURLES⁸, AND PHILIP J. MARSHALL¹*Draft version February 9, 2022*

ABSTRACT

We report the discovery of two concentric partial Einstein rings around the gravitational lens SDSSJ0946+1006, as part of the Sloan Lens ACS Survey. The main lens is at redshift $z_1 = 0.222$, while the inner ring (1) is at redshift $z_{s1} = 0.609$ and Einstein radius $R_{\text{Ein}1} = 1.43 \pm 0.01''$. The wider image separation ($R_{\text{Ein}2} = 2.07 \pm 0.02''$) of the outer ring (2) implies that it is at higher redshift than Ring 1. Although no spectroscopic feature was detected in ~ 9 hours of spectroscopy at the Keck I Telescope, the detection of Ring 2 in the F814W ACS filter implies an upper limit on the redshift of $z_{s2} \lesssim 6.9$. The lens configuration can be well described by a power law total mass density profile for the main lens $\rho_{\text{tot}} \propto r^{-\gamma'}$ with logarithmic slope $\gamma' = 2.00 \pm 0.03$ (i.e. close to isothermal), velocity dispersion $\sigma_{\text{SIE}} = 287 \pm 5 \text{ km s}^{-1}$ (in good agreement with the stellar velocity dispersion $\sigma_{v,*} = 284 \pm 24 \text{ km s}^{-1}$) with little dependence upon cosmological parameters or the redshift of Ring 2. Using strong lensing constraints only we show that the enclosed mass to light ratio increases as a function of radius, inconsistent with mass following light. Adopting a prior on the stellar mass to light ratio from previous SLACS work we infer that $73 \pm 9\%$ of the mass is in form of dark matter within the cylinder of radius equal to the effective radius of the lens. We consider whether the double source plane configuration can be used to constrain cosmological parameters exploiting the ratios of angular distance ratios entering the set of lens equations. We find that constraints for SDSSJ0946+1006 are uninteresting due to the sub-optimal lens and source redshifts for this application. We then consider the perturbing effect of the mass associated with Ring 1 (modeled as a singular isothermal sphere) building a double lens plane compound lens model. This introduces minor changes to the mass of the main lens, allows to estimate the redshift of the Ring 2 ($z_{s2} = 3.1^{+2.0}_{-1.0}$), and the mass of the source responsible for Ring 1 ($\sigma_{\text{SIE},s1} = 94^{+27}_{-47} \text{ km s}^{-1}$). We conclude by examining the prospects of doing cosmography with a sample of 50 double source plane gravitational lenses, expected from future space based surveys such as DUNE or JDEM. Taking full account of the uncertainty in the mass density profile of the main lens, and of the effect of the perturber, and assuming known redshifts for both sources, we find that such a sample could be used to measure Ω_m and w with 10% accuracy, assuming a flat cosmological model.

Subject headings: Gravitational lensing – galaxies : Ellipticals and lenticulars, cD – galaxies: structure
– galaxies: halos – cosmology: dark matter – cosmology: cosmological parameters

1. INTRODUCTION

Electronic address: gavazzi@iap.fr

[†] Based on observations made with the NASA/ESA Hubble Space Telescope, obtained at the Space Telescope Science Institute, which is operated by the Association of Universities for Research in Astronomy, Inc., under NASA contract NAS 5-26555. These observations are associated with program #10886. Support for program #10886 was provided by NASA through a grant from the Space Telescope Science Institute, which is operated by the Association of Universities for Research in Astronomy, Inc., under NASA contract NAS 5-26555.

¹ Department of Physics, University of California, Broida Hall, Santa Barbara, CA 93106-9530, USA

² Sloan Fellow

³ Packard Fellow

⁴ Kapteyn Astronomical Institute, University of Groningen, PO box 800, 9700 AV Groningen, The Netherlands

⁵ Institute for Astronomy, University of Hawaii, 2680 Wodlawn Dr., Honolulu, HI 96822, USA

⁶ Harvard-Smithsonian Center for Astrophysics, 60 Garden St. MS-20, Cambridge, MA 02138, USA

⁷ Jet Propulsion Laboratory, Caltech, MS 169-327, 4800 Oak Grove Dr., Pasadena, CA 91109, USA

⁸ Department of Physics and Kavli Institute for Astrophysics and Space Research, Massachusetts Institute of Technology, 77 Massachusetts Ave., Cambridge, MA 02139, USA

Measuring the mass distribution of galaxies is essential for understanding a variety of astrophysical processes. Extended mass profiles of galaxies provide evidence for dark matter either using rotation curves (*e.g.* Rubin et al. 1980; van Albada et al. 1985; Swaters et al. 2003), weak lensing (*e.g.* Brainerd et al. 1996; Hoekstra et al. 2004; Sheldon et al. 2004; Mandelbaum et al. 2006), or dynamics of satellite galaxies (*e.g.* Prada et al. 2003; Conroy et al. 2007) which is one of the main ingredients of the standard Λ cold dark matter (Λ CDM) cosmological model. At galactic and subgalactic scales, numerical cosmological simulations make quantitative predictions regarding, *e.g.*, the inner slope of mass density profiles and the existence of dark matter substructure. Precise mass measurements are key to test the predictions and provide empirical input to further improve the models.

Gravitational lensing has emerged in the last two decades as one of the most powerful ways to measure the mass distributions of galaxies, by itself or in combination with other diagnostics. Although strong gravitational lenses are relatively rare in the sky ($\lesssim 20$ per square degree at space-based depth and resolution; Marshall et al. 2005; Moustakas et al. 2007), the number

of known galaxy-scale gravitational lens systems has increased well beyond a hundred as a result of a number of dedicated efforts exploiting a variety of techniques (*e.g.* Warren et al. 1996; Ratnatunga et al. 1999; Kochanek et al. 1999; Myers et al. 2003; Bolton et al. 2004; Cabanac et al. 2007). The increased number of systems, together with the improvement of modeling techniques (*e.g.* Kochanek & Narayan 1992; Warren & Dye 2003; Treu & Koopmans 2004; Brewer & Lewis 2006; Suyu et al. 2006; Wayth & Webster 2006; Barnabè & Koopmans 2007), has not only enabled considerable progress in the use of this diagnostic for the study of the mass distribution of early and most recently late-type galaxies, but also for cosmography, i.e. the determination of cosmological parameters (*e.g.* Golse et al. 2002; Soucaill et al. 2004; Dalal et al. 2005).

Given the already small optical depth for strong lensing, the lensing of multiple background sources by a single foreground galaxy is an extremely rare event. At Hubble Space Telescope (HST) resolution (FWHM $\sim 0''.12$) and depth ($I_{AB} \sim 27$) it is expected that one massive early-type galaxy (which dominate the lensing cross-section) in about 200 is a strong lens (Marshall et al. 2005). Taking into account the strong dependence of the lensing cross-section on lens galaxy velocity dispersion ($\propto \sigma^4$), and the population of lens galaxies, we estimate that about one lens galaxy in $\sim 40 - 80$ could be a double source plane strong gravitational lens (see appendix A). For these reasons, at most a handful of double lenses are to be found in the largest spectroscopic surveys of early-type galaxies such as the luminous red galaxies of the Sloan Digital Sky Survey. However, future high resolution imaging surveys such as those planned for JDEM and DUNE (Aldering & the SNAP collaboration 2004; Réfrégier et al. 2006) will increase the number of known lenses by 2-3 orders of magnitude (Marshall et al. 2005), and hence should be able to provide large statistical samples of double source plane gravitational lenses, opening up the possibility of qualitatively new applications of gravitational lensing for the study of galaxy formation and cosmography.

We report here the discovery of the first double source plane partial Einstein Ring. The gravitational lens system SDSSJ0946+1006, was discovered as part of the Sloan Lens ACS (SLACS) Survey (Bolton et al. 2005, 2006a; Treu et al. 2006; Koopmans et al. 2006; Bolton et al. 2007; Gavazzi et al. 2007). The object was first selected by the presence of multiple emission lines at higher redshift in the residuals of an absorption line spectrum from the SDSS database as described by Bolton et al. (2004) and then confirmed as a strong lens by high resolution imaging with the Advanced Camera for Surveys aboard HST. In addition to an Einstein ring due to the source (hereafter source 1) responsible for the emission lines detected in the SDSS spectrum, the Hubble image also shows a second multiply imaged system forming a broken Einstein Ring with a larger diameter than the inner ring (hereafter source 2). This configuration can only arise if the two lensed systems are at different redshifts and well aligned with the center of the lensing galaxy. It is a great opportunity that a double source plane lens has been found among the approximately 90 lenses discovered by the SLACS collaboration to date (Bolton et al. 2008, in prep.).

The goal of this paper is to study and model this peculiar system in detail, as an illustration of some astrophysical applications of double source plane compound lenses, including i) the determination of the mass density profile of the lens galaxy independent of dynamical constraints; ii) placing limits on the mass of source 1 based on multiple lens plane modeling; iii) estimating the redshift of source 2 and the cosmological parameters from the angular distance size ratios. The paper is therefore organized as follows. Section 2 summarizes the observations, photometric and spectroscopic measurements, and discusses the morphology of the lens system. Section 3 describes our gravitational lens modeling methodology. Section 4 gives the main results in terms of constraints on the mass distribution of the lens galaxy and of source 1. Section 5 discusses the use of double source plane lenses as a tool for cosmography using the example of SDSSJ0946+1006 and also addresses the potential of large samples of such double source plane lenses for the same purpose. In section 6 we summarize our results and briefly conclude.

Unless otherwise stated we assume a concordance cosmology with $H_0 = 70 h_{70} \text{ km s}^{-1} \text{ Mpc}^{-1}$, $\Omega_m = 0.3$ and $\Omega_\Lambda = 0.7$. All magnitudes are expressed in the AB system.

2. DATA

The lens galaxy SDSSJ0946+1006 was first identified in the spectroscopic SDSS database based on the redshift of the lensing galaxy $z_l = 0.222$ and that of a background source at $z_{s1} = 0.609$ (hereafter source 1), as described by Bolton et al. (2004, 2006a), and Bolton et al. (2008, in prep.). This section describes HST follow-up imaging (§2.1), the properties of the lens (§2.2) and lensed (§2.3) galaxies.

2.1. Hubble Space Telescope observations & data reduction

SDSSJ0946+1006 was then imaged with the ACS on board the HST (cycle 15, Prog. 10886, PI Bolton). The Wide Field Channel with filter F814W was used for a total exposure time of 2096 s. Four sub-exposures were obtained with a semi-integer pixel offset (`acs-wfc-dither-box`) to ensure proper cosmic ray removal and sampling of the point spread function. The image reduction process is described in (Gavazzi et al. 2007) and results in a $0''.03/\text{pixel}$ spatial sampling. This pixel size provides good sampling of the PSF for weak lensing applications, at the (small) price of inducing noise correlation over scales of 1-2 pixels. This is accounted for in our analysis by correcting pixel variances according to the procedure described by Casertano et al. (2000).

Figure 1 shows the HST image of the lens galaxy field together with an enlarged view of the lensed features, after subtraction of a smooth model for the lens surface brightness distribution. For reference, one arcsecond in the lens plane subtends a physical scale of $3.580 h_{70}^{-1} \text{ kpc}$.

2.2. Lens galaxy properties

The two-dimensional lens surface brightness was fitted with `galfit` (Peng et al. 2002) using two elliptical Sérsic components. The addition of a second component is needed to provide a good fit in the center, and to reproduce the isophotal twist in the outer regions. To reduce

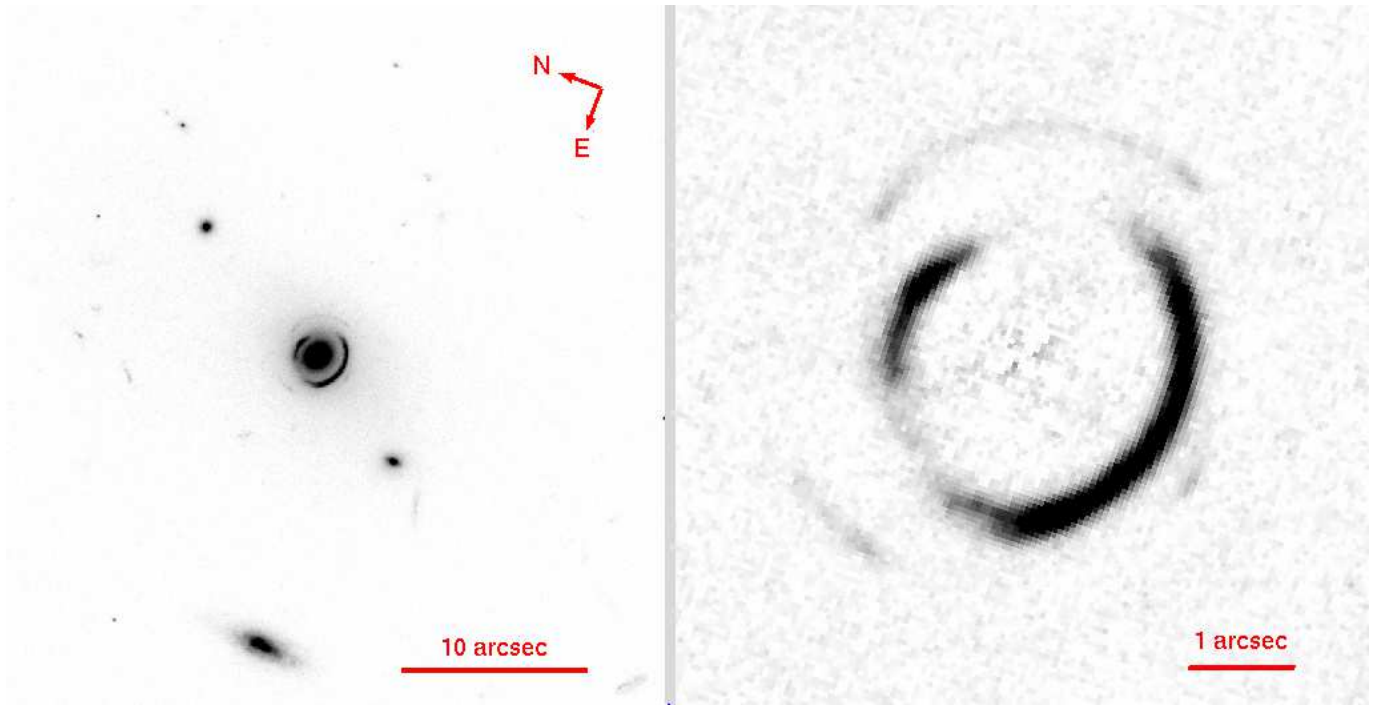


FIG. 1.— HST/F814W overview of the lens system SDSSJ0946+1006. The right panel is a zoom onto the lens showing two concentric partial ring-like structures after subtracting the lens surface brightness.

the effect of lensed features in the fit we proceeded iteratively. We first masked the lensed features manually, then we performed *galfit* fits creating masks by 4σ clipping. Two iterations were needed to achieve convergence.

The total magnitude of the lens obtained by summing the flux of the two Sérsic models is $F814W = 17.110 \pm 0.002$ after correction for Galactic extinction (Schlegel et al. 1998). The rest-frame V band absolute magnitude is $M_V = -22.286 \pm 0.025$ using the K-correction of Treu et al. (2006). The errors are dominated by systematic uncertainties on the K-correction term. The most concentrated Sérsic component c_1 dominates at the center and accounts for about 17.5% of the total lens flux. The effective radius of c_1 is about $0.4''$ whereas that of c_2 is $\sim 3''$ with about 10% relative accuracy. Similarly, the Sérsic indexes are $n_{c_1} \simeq 1.23$ and $n_{c_2} \simeq 1.75$.

To measure the one dimensional light profile of the lens galaxy, we used the IRAF task *ellipse*. Fig. 2 shows the radial change of ellipticity and position angle of the light distribution. There is a clear indication of a sharp change in position angle and ellipticity between $1-2''$. This isophotal twist is well captured by the double Sérsic profile fit, that requires different PAs for the two components. Therefore we conclude that the lens galaxy is made of two misaligned components, having similar surface brightness at radius $\sim 0.6''$.

For comparison, a single component Sérsic fit yields $n \simeq 3.73$, consistent with the typical light profiles of massive early-type galaxies. The effective radius of the composite surface brightness distribution is found to be $R_{\text{eff}} = 2.02 \pm 0.10 \text{ arcsec} \simeq 7.29 \pm 0.37 h_{70}^{-1} \text{ kpc}$, where we assumed a typical relative uncertainty of about 5% as discussed in (Treu et al. 2006). It is also consistent with an independent measurement reported by Bolton

et al. (2008, in prep.) who considered de Vaucouleurs surface brightness distributions ($n \equiv 4$ by construction). Note that we use the same convention for all characteristic radii reported throughout. For elliptical distributions radii are expressed at the intermediate radius (*i.e.* the geometric mean radius $r = \sqrt{ab}$).

In addition, the stellar velocity dispersion $\sigma_{\text{ap}} = 263 \pm 21 \text{ km s}^{-1}$ was measured with SDSS spectroscopy within a $3''$ diameter fiber. We convert this velocity dispersion σ_{ap} into the fiducial velocity $\sigma_{v,*}$ that enters Fundamental Plane analyses and measured in an aperture of size $R_{\text{eff}}/8$ using the relation $\sigma_{v,*}/\sigma_{\text{ap}} = (R_{\text{eff}}/8/R_{\text{ap}})^{-0.04} \simeq 1.08$ (see Treu et al. 2006, and references therein).

Based on photometric redshifts available online on the SDSS webpage (Oyaizu et al. 2007), we note that the lens galaxy is the brightest galaxy in its neighborhood. Another bright galaxy about 40 arcsec south-west of SDSSJ0946+1006 exhibits perturbed isophotes (an extended plume) suggesting that it may have flown by recently and might end up merging onto the lens galaxy. Its photometric redshift is $z_{\text{phot}} = 0.20 \pm 0.04$ consistent with SDSSJ0946+1006 redshift. The extended envelope captured by the double Sérsic component fit also supports the recent flyby hypothesis (*e.g.* Bell et al. 2006).

2.3. Lensed structures

Two concentric partial ring-like structures are clearly seen at radii $1.43 \pm 0.01''$ and $2.07 \pm 0.02''$ from the center of the lens galaxy (Figure 1). Such a peculiar lensing configuration – with widely different image separations of nearly concentric multiple image systems – implies that the rings come from two sources at different redshift, the innermost (Ring 1) corresponding to the nearest background source 1 and the outermost (Ring 2) being significantly further away along the optical axis.

Ring 1 has a typical cusp configuration with 3 merg-

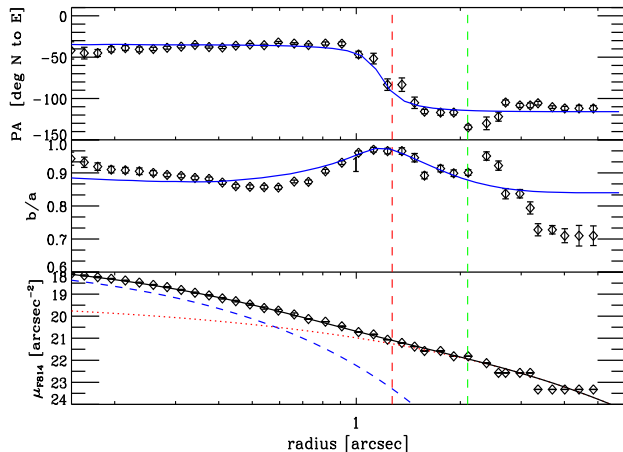


FIG. 2.— Results for isophotal fit with *IRAF/ellipse*. *Top panel*: Position angle versus radius. *Middle panel*: Axis ratio versus radius. The vertical lines show the location of the inner and outer Einstein rings which were masked out during the fitting process. We also overlay in the top and middle panels as a blue solid line the *ellipse* output performed on the best fit *galfit* two-dimensional brightness distribution. *Bottom panel*: best fit Sérsic profiles obtained with *galfit*. The formal error bars on the surface brightness profile are smaller than the data points.

ing conjugate images and a counterimage on the opposite side of the lens and closer to the center than the large cusp “arc”. This constrains the orientation of the lens potential major axis to pass almost through the middle of both arcs. Ring 1 is among the brightest ones to have been discovered in the SLACS survey (See Bolton et al. 2008, in prep., for the latest compilation). The observed F814W magnitude is $m_1 = 19.784 \pm 0.006$ (extinction corrected). The error bar includes only statistical uncertainties. An additional systematic error of order $\lesssim 0.1$ mag is likely present due to uncertainties in the lens galaxy subtraction (Marshall et al. 2007).

Ring 2 presents a nearly symmetrical Einstein cross configuration (with a faint bridge between the north and west images), implying that the source must lie very close to the optical axis. The observed F814W magnitude is $m_2 = 23.68 \pm 0.09$, making it about 36 times fainter than Ring 1. As for Ring 1 the error bar includes only statistical uncertainties.

No evidence of Ring 2 is present in the SDSS spectrum. This can be explained by the low peak surface brightness of Ring 2 (~ 23 mag arcsec $^{-2}$) and less importantly by the diameter of the second ring being slightly larger than the $3''$ SDSS fiber (although see Bolton et al. 2006b, for a successful redshift measurement in a similar case). Deeper longslit spectroscopy was obtained at Keck Observatory with the Low Resolution Imager Spectrograph (LRIS) instrument on December 22-23 2006, the total integration time being about 9 hours. The goal was two-fold: i) obtain the redshift of Ring 2; ii) measure the stellar velocity dispersion profile of the main lens. This latter aspect will be presented elsewhere. Despite the large integration time, we could not measure the source redshift z_{s2} due to a lack of emission lines in the range $[3500, 8600\text{\AA}]$ that do not belong to Ring 1. Since Ring

2 is detected in the ACS/F814W filter, we can set an upper limit on its redshift $z_{s2} < 6.9$ by requiring that the Lyman break be at shorter wavelengths than the red cutoff of the filter.

3. LENS MODELING

3.1. Model definition

This section describes our adopted strategy to model this exceptional lens system. We begin with a simplifying assumption. Although the gravitational potential arises from both a stellar and a dark matter component, a single power law model for the total density profile turns out to be a good description of SLACS lenses (Koopmans et al. 2006). Therefore, we assume the total convergence for a source at redshift z_s to be of the form:

$$\kappa(\vec{r}, z_s) = \frac{b_\infty^{\gamma'-1}}{2} (x^2 + y^2/q^2)^{(1-\gamma')/2} \frac{D_{ls}}{D_{os}}, \quad (1)$$

with 4 free parameters: the overall normalization b , the logarithmic slope of the density profile γ' , the axis ratio q and position angle PA_0 (omitted in Eq. (1) for simplicity) of iso- κ ellipses. The familiar case of the singular isothermal sphere is that corresponding to a slope $\gamma' = 2$ and $q = 1$. In this case b_∞ relates to the velocity dispersion of the isothermal profile by $b_\infty = 4\pi(\sigma_{SIE}/c)^2 = (\sigma_{SIE}/186.2 \text{ km s}^{-1})^2 \text{ arcsec}$. Note that σ_{SIE} is nothing but a way of redefining the normalization of the convergence profile and does not necessarily correspond in a straightforward sense to the velocity dispersion of stars in the lens galaxy. In general, for every combination of model parameters, the stellar velocity dispersion of a specified tracer embedded in the potential can be computed by solving the Jeans equation and will be a function of radius and observational effects such as aperture and seeing.

No assumptions are made about the orientation of the position angle PA_0 of the lens potential. In addition, we allow for external shear with modulus γ_{ext} and position angle PA_{ext} . For a multiple source plane system, it is necessary to define a lens plane from which the external shear comes from since shear has to be scaled by the appropriate D_{ls}/D_{os} term for each source plane. For simplicity we assume that the global effect of external perturbations comes from the same lens plane $z_1 = 0.222$. We expect a strong degeneracy between internal ellipticity and external shear but include this extra degree of freedom in the model to account for any putative twist of isopotentials, as suggested by the observed isophotal twist in the lens galaxy surface brightness. Note also that the need of being able to handle two distinct source planes led us to the somewhat unusual definition of b_∞ in Eq. (1). With this convention, $(b_\infty \sqrt{q})^{\gamma'-1} D_{ls}/D_{os}$ is the quantity closest to the b_{SIE} (or R_{Einst}) parameter used in other SLACS papers (Koopmans et al. 2006; Bolton et al. 2008). Note also that the center of mass is assumed to match exactly the lens galaxy center of light. The unknown redshift of source 2 is also treated as a free parameter, for which we assign a uniform $1 \leq z_{s2} \leq 6.9$ prior. Altogether, we use 7 free parameters to characterize the potential of SDSSJ0946+1006: b_∞ , γ' , q , PA_0 , γ_{ext} , PA_{ext} and z_{s2} .

In this section and the next, we neglect the extra focusing effect of Ring 1 acting as a lens on Ring 2, leaving the discussion of this perturber for Section 5.

3.2. Methods

We consider three strategies for studying gravitational lens systems with spatially resolved multiple images.

The first one consists of identifying conjugate bright spots in the multiple images and minimizing the distance of conjugate points in the source plane. This approach is statistically conservative in the sense that it only takes partial advantage of the large amount of information present in the deep HST data. However, it has the benefit of being robust and relatively insensitive to the details of the source morphology, and other concerns that affect different alternative techniques in the case.

The second approach is the linear source inversion and parametric potential fitting method described by Warren & Dye (2003), Treu & Koopmans (2004), Koopmans (2005) and Suyu et al. (2006). A strong advantage of this method is that it takes fully into account the amount of information contained in each pixel. Although this method is robust, there are many degrees of freedom to model the intrinsic source surface brightness distribution and thus some form of regularisation is needed to avoid fitting the noise as described in the references above.

The third method (*e.g.* Marshall et al. 2007; Bolton et al. 2007, 2008) describes the source as one or several components parameterized with elliptical surface brightness profiles (usually Sérsic). In general, this method provides good fits to the data as long as not too many such components are needed to represent the source, and directly provides physically meaningful parameters for the source. For high signal-to-noise ratio images of complex lensed features the dimensionality of the problem may increase very fast.

In the case of a multiple source plane system, two difficulties arise when using the second and third techniques. 1) Our current pixellized method does not handle multiple source planes (see *e.g.* Dye et al. 2007, for recent progress along this line). 2) The statistical weight given to each of the partial rings depends essentially on their relative brightness. Since Ring 1 is 36 times brighter than Ring 2, it completely dominates the fit. This has the unwanted side effect that a physically uninteresting morphological mismatch of the inner ring, due for example to poor modeling of the source or of the point spread function, overwhelms any mismatch in the physically important *image separation* of the outer ring.

The goal of the present analysis is to confirm that SDSSJ0946+1006 is the first example of a galaxy-scale double source plane system and illustrate what kind of information can be inferred from such a configuration. After experimenting with all three techniques – and in light of the difficulties described above – we decided to focus on the more straightforward conjugate points modeling technique, using the other techniques to aid in our modeling.

In practice, the modeling technique adopted here is similar to the one used by Gavazzi et al. (2003). The merging cusp nature of ring 1 makes the identification of quadruply imaged spots hazardous along the elongated arc but identifications are much easier between the opposite counter-image and the elongated arc. The identification of the brightness peak S2 in Ring 2 is obvious. To guide the identification process, we also used fits based on the pixellized source inversion. We ended up having

4 spots identified in Ring 1, two of them having 3 clear conjugations (S1a, S1c) whereas the other two have only have 2 (S1b, S1d). One single bright spot in Ring 2 is imaged 4 times. The typical rms error made on the location of spots estimated to be $0.03''$. Table 1 summarizes the coordinates of matched points in the same frame as Fig. 1. For each knot S1a, S1b, S1c, S1d and S2, multiple images with positive parity have an odd labelling number. To guide the fitting procedure we also demand the image parity to be preserved by the model. Therefore, taking into account the unknown position of these spots in the source plane, we end up having 18 constraints (see Gavazzi et al. 2003) whereas the considered model has 7 free parameters. Hence the optimization problem has 11 degrees of freedom.

TABLE 1
SUMMARY OF PIXEL COORDINATES USED FOR LENS MODELING.

| | Img. 1 | Img. 2 | Img. 3 | Img. 4 |
|-----|--------------|-------------|------------|-------------|
| S1a | 0.34, -1.50 | -0.94, 0.68 | 1.52, 0.19 | – |
| S1b | – | -1.16, 0.22 | 1.44, 0.88 | – |
| S1c | -0.43, -1.42 | -1.10, 0.67 | 1.23, 0.88 | – |
| S1d | -0.14, -1.68 | -0.57, 0.96 | – | – |
| S2 | -1.51, -1.78 | 1.56, -1.19 | 1.55, 1.65 | -1.34, 1.32 |

Positions (x,y) of each multiple knot are expressed in arcsec (typical rms error $0.03''$) relative to the lens galaxy surface brightness peak (got from *galfit* modeling, see §2.2). The frame position angle is 161.348° relative to North direction.

4. MODELING RESULTS

The optimization process and the exploration of the parameter space were performed by sampling the posterior probability distribution function with Monte-Carlo Markov Chains (MCMC). We assumed flat priors. Table 2 summarizes the results (“best fit” values are defined as the median value of the marginalized PDF) and their corresponding 68% CL uncertainties after marginalizing the posterior over all the other parameters. The best fit model yields a $\chi^2/\text{dof} = 13.2/11 \simeq 1.20$ which is statistically reasonable¹⁰.

TABLE 2
BEST-FIT MODEL PARAMETERS FOR SDSSJ0946+1006 USING A SINGLE LENS PLANE.

| | |
|---------------------------------------------|----------------------------|
| b_∞ [arcsec] | 2.54 ± 0.09 |
| γ' | 2.00 ± 0.03 |
| axis ratio q | $0.869^{+0.017}_{-0.013}$ |
| PA_0 | $-11.8^{+7.0}_{-8.9}$ |
| γ_{ext} | $0.067^{+0.010}_{-0.007}$ |
| PA_{ext} | $-31.5^{+6.9}_{-4.8}$ |
| z_{s2} | $5.30^{+1.03}_{-1.00}$ |
| σ_{SIE} [km s ⁻¹] | $287.0^{+5.1}_{-5.3}$ |
| “unlensed” apparent $F814_{s1}$ [mag] | $22.76 \pm 0.02 \pm 0.10$ |
| “unlensed” absolute V_{s1} [mag] | $-19.79 \pm 0.05 \pm 0.10$ |
| “unlensed” apparent $F814_{s2}$ [mag] | $27.01 \pm 0.09 \pm 0.10$ |

Best fit model parameters and 68.4% confidence limits. Errors on magnitudes distinguish statistical (first) and systematic from lens light subtraction (second). Angles are in degrees oriented from North to East.

¹⁰ A χ^2 distribution with 11 degrees of freedom gives a probability of 28% that the χ^2 value will be greater than 13.2.

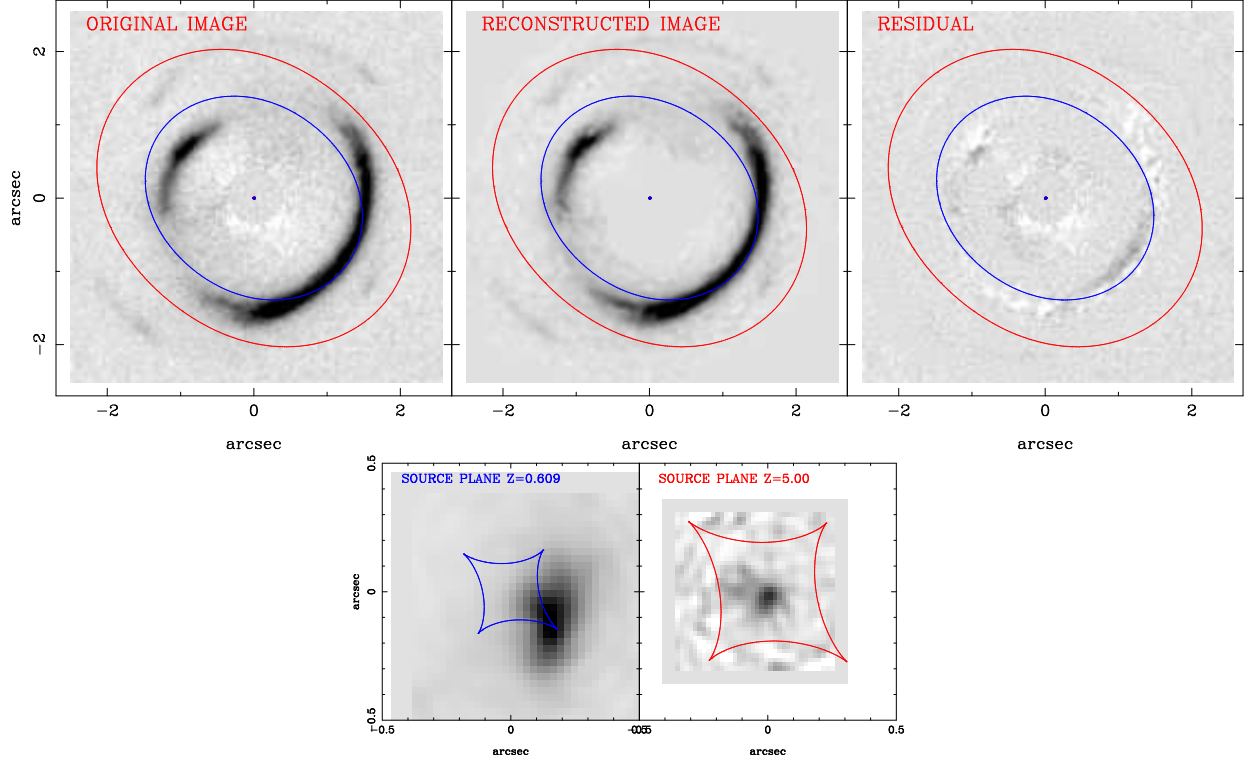


FIG. 3.— Best-fit single lens plane model for the lens SDSSJ0946+1006. The model parameters were found using the identification of conjugate bright knots but the quality of the model is illustrated with a pixelised source inversion technique. *Top left*: observation with the lens light profile subtracted off. *Top middle*: model prediction in the image plane and associated residuals (*Top right*). The model also predicts the light distribution in the source planes z_{s1} and z_{s2} (*Bottom left and right* respectively). Note a different color stretching for source plane 2 (factor 6) in this latter case. Critical and caustic lines corresponding to the two source planes are overlaid (smaller blue for $z_{s1} = 0.609$ and wider red for $z_{s2} = 5$).

The results of the best fit model inferred from the conjugation of bright spots is shown in Fig. 3 where we used the pixelized source inversion technique to illustrate the quality of the fit and the reliability of the conjugation method. Although the surface brightness of Ring 1 and Ring 2 identified by separate annuli in the image plane are inverted separately, model predictions in the image plane are recombined for convenience. The two source planes $z_{s1} = 0.609$ and $z_{s2} \simeq 5$ are also shown.

As expected, there is a degeneracy between external shear and ellipticity of the total mass distribution and the modeling, suggesting that the major axis of the potential and the external shear differ by $PA_0 - PA_{\text{ext}} = 20^{+12}_{-16}$ deg, that is they are aligned within $\sim 1.2\sigma$. The orientation of external shear in agreement with the orientation of stars out to $r \lesssim 1''$ which is about -36 deg. The orientation of the internal quadrupole (lens ellipticity) and that of stars are misaligned by $\sim 24^\circ$. Likewise, the axis ratio of the light distribution over this radial range is $0.85 \lesssim b/a \lesssim 0.93$, again consistent with our lens model.

The lens modeling also puts interesting constraints on the redshift of source 2: $z_{s2} = 5.3 \pm 1.0$. The accuracy is relatively low because of the saturation of the $D_{\text{ls}}/D_{\text{os}}(z_s)$ curve when $z_s \rightarrow \infty$. The top panel of Fig. 4 shows a mild correlation between z_{s2} and the slope of the density profile γ' . This is expected since the steeper the density profile that fits the inner ring, the less mass is enclosed between the two rings, and hence the further away must be the outer source.

In spite of the complexity of the azimuthal properties of the lens potential, our modeling yielded stable and

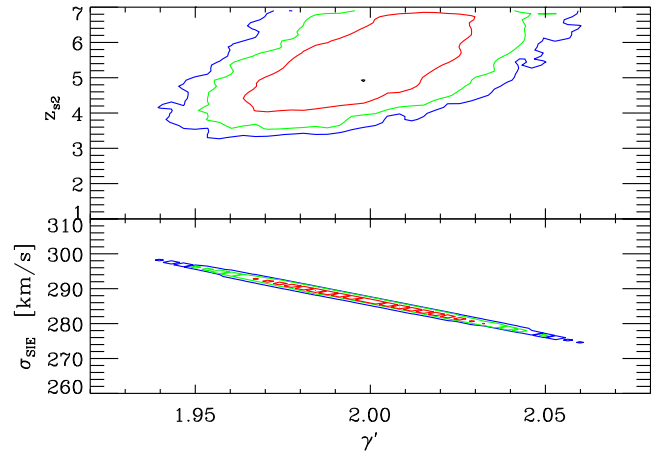


FIG. 4.— *Top panel*: 68.3%, 95.4% and 99.3% CL contours for model parameters slope of the density profile γ' and source 2 redshift z_{s2} . *Bottom panel*: *Idem* for the slope γ' and the lens equivalent velocity dispersion (defined as $186.2\sqrt{b_\infty q^{1/2}/1''} \text{ km s}^{-1}$).

well localized constraints on the normalization and slope of the radial total density profile. The lower panel of Fig. 4 shows the confidence regions for the slope γ' and the equivalent velocity dispersion σ_{SIE} . First, we find a total density profile very close to isothermal with a slope $\gamma' = 2.00 \pm 0.03$. The corresponding SIE velocity dispersion is $\sigma_{\text{SIE}} = 287.0 \pm 5.2 \text{ km s}^{-1}$. In order to compare these results with SDSS spectroscopy, one needs to solve the spherical Jeans equation taking into account observa-

tional effects (SDSS fiber aperture, seeing) and the surface density of dynamical tracers (radial distribution of stars in the lens galaxy) measured in §2.2. Here we assume an isotropic pressure tensor. A general description of the method can be found in Koopmans (2006). Fig. 5 shows the aperture velocity dispersion that would be measured with SDSS spectroscopic fibers when the density profile is normalized to fit the first ring alone. It shows that slopes close to isothermal ($\gamma' \simeq 2$) predict velocity dispersions close to SDSS spectroscopic velocity dispersion, which gives strong support to our double source plane lensing-only analysis. Such a similarity is consistent with the results of previous SLACS studies (Treu et al. 2006; Koopmans et al. 2006). We note that the accuracy reached on both the slope and the velocity dispersion based on lensing constraints alone is better than that afforded by kinematical measurements at the same redshift, although the two methods are complementary in their systematic errors and degeneracies (see discussion in *e.g.* Treu & Koopmans 2002).

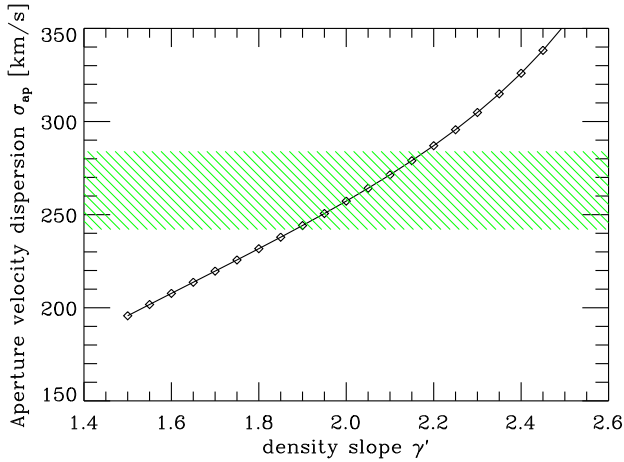


FIG. 5.— Predicted stellar aperture velocity dispersion σ_{ap} as it would be measured with SDSS spectroscopic settings as a function of the slope of the density profile. The normalization of density profile is fixed to be consistent with the Einstein radius of Ring 1. The shaded area is the 1σ SDSS measurement uncertainty. It shows a remarkable agreement between the double source plane analysis and the coupling of kinematical + source 1 plane data, both favoring nearly isothermal slopes. Note that σ_{ap} and σ_{SIE} do not need to be identical.

4.1. Budget of mass and light in SDSSJ0946+1006

The tight constraints on the projected mass profile between the two Einstein radii can be compared to the light distribution inferred in §2.2. In particular, the total projected V band mass-to-light ratio within the effective radius $R_{\text{eff}} \simeq 7.29 h_{70}^{-1} \text{ kpc}$ is $M/L_V = 11.54 \pm 0.51 h_{70} (M/L_V)_{\odot}$ (corresponding to a total projected mass $4.90 \pm 0.13 \times 10^{11} h_{70}^{-1} M_{\odot}$). The logarithmic slope of the projected enclosed total mass profile is $3 - \gamma' = 1.00 \pm 0.03$, while the slope of the cumulative luminosity profile close to the effective radius is $d \log L(< r)/d \log r = 0.62$ with much smaller uncertainty. Therefore the projected mass-to-light ratio profile increases with radius as $r^{0.38 \pm 0.03}$ around R_{eff} with high statistical significance.

We now compare these values to the stellar mass content in the effective radius using a the typical mass-to-light ratio of stellar populations in massive galaxies at that redshift $M_*/L_V \simeq 3.14 \pm 0.32 h_{70} (M/L_V)_{\odot}$ (Gavazzi et al. 2007) and $\sim 30\%$ intrinsic scatter about this values (due to *e.g.* age-metallicity effects) as found in the local Universe (Gerhard et al. 2001; Trujillo et al. 2004). This leads to a fraction of projected mass in the form of dark matter within the effective radius $f_{\text{DM},2D}(< R_{\text{eff}}) \simeq 73 \pm 9\%$ which is about twice as high as the average value found by Gavazzi et al. (2007) and Koopmans et al. (2006) thus making SDSSJ0946+1006 a particularly dark-matter-rich system.

5. EXPLOITING THE DOUBLE SOURCE PLANE: BEYOND THE LENS MASS PROPERTIES

In this section we address two particular applications afforded by the double source plane nature of SDSSJ0946+1006. First, in §5.1 we discuss whether this particular system gives interesting constraints on cosmological parameters. Then, in §5.2, we present a compound double lens plane mass model and use it to constrain the total mass of the Ring 1. This provides a new (and perhaps unique) way to obtain total masses of such compact and faint objects. Thus, in combination with the magnifying power of the main lens, this application appears to be a promising way to shed light on the nature of faint blue compact galaxies (*e.g.* Marshall et al. 2007). In § 5.3 we discuss the prospects of doing cosmography with samples of double source plane lenses, taking into account the lensing effects of the inner ring on the outer ring.

5.1. An ideal optical bench for cosmography?

Can a double source plane lens be used to constrain global cosmological parameters like Ω_m or Ω_{Λ} ? In principle this can be done because lensing efficiency depends on the ratio of angular diameter distances to the source D_{os} and between the lens and the source D_{ls} as well as the projected surface mass density $\Sigma(\vec{\theta})$ in the lens plane. In formulae, writing the lens potential experienced by light rays coming from a source plane as redshift z_s as:

$$\psi(\vec{\theta}, z_s) = \frac{4G}{c^2} \frac{D_{\text{ol}} D_{\text{ls}}}{D_{\text{os}}} \int d^2 \theta' \Sigma(\vec{\theta}') \ln |\vec{\theta} - \vec{\theta}'| \quad (2)$$

$$\equiv \psi_0(\vec{\theta}) \frac{D_{\text{ls}}}{D_{\text{os}}}, \quad (3)$$

and considering two images at positions $\vec{\theta}_1$ and $\vec{\theta}_2$ coming from source planes at redshift z_{s1} and z_{s2} , one can measure the ratio of distance ratios $\eta \equiv (D_{\text{ls}}/D_{\text{os}})_{z_{s2}} / (D_{\text{ls}}/D_{\text{os}})_{z_{s1}}$ directly from the properties of the multiple images, given assumptions on the potential $\psi_0(\vec{\theta})$ and its derivatives defining the deflection, convergence and shear at the positions of the images.

Applications of this method to clusters of galaxies with several multiply imaged systems at different source redshifts – assuming simple parametric models for the clusters – seem to favor $\Omega_m < 0.5$ cosmologies (Golse et al. 2002; Soucaill et al. 2004). However, unknown systematics lurk under the cluster substructure, which can introduce significant local perturbations of $\psi_0(\vec{\theta})$. In principle – at least judging qualitatively from the smoothness of

the isophotes, and the smoothness of galaxy scale Einstein Rings – one could hope that massive elliptical galaxies be less prone to this sort of systematic because source size is large compared to the substructure angular scale.

In the previous section we constrained z_{s2} for the given Λ CDM concordance cosmology. Here we re-parametrize the problem using η itself as a free parameter to constrain the change in lensing efficiency between the two source planes. The left panel of Fig. 6 shows the joint constraints on the two parameters γ' and η . A first consequence of this more general parameterization is that, by allowing a broader range of values for η (i.e. allowing more freedom in the cosmological model), the uncertainties on the slope are significantly increased: we find $\gamma' = 2.07 \pm 0.06$. Steeper density profiles are now somewhat compensated by a relatively higher lensing efficiency for the second source plane. In other words, the tight constraints previously obtained on the slope of the density profile depend to some extent on the assumed cosmological model (i.e. assuming Λ CDM cosmology led to $\gamma' = 2.00 \pm 0.03$).

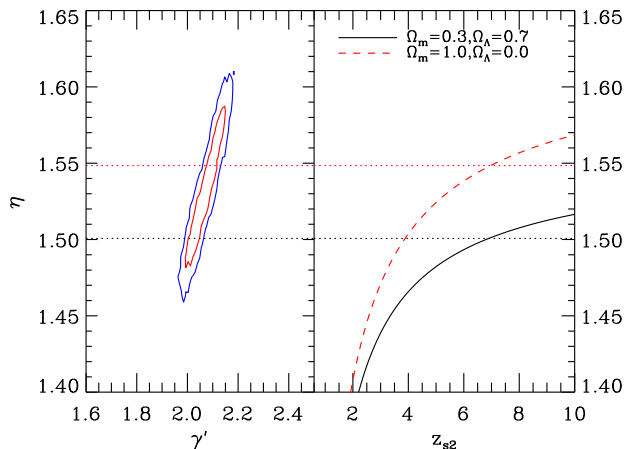


FIG. 6.— *Left panel:* Constraints on the logarithmic slope γ' and the ratio of distance ratios η . Contours enclose 68.3% and 95.4% of probability. The *right panel* shows $\eta(z_{s2})$ as a function of z_{s2} for two flat cosmologies $(\Omega_m, \Omega_\Lambda) = (0.3, 0.7)$ (black) and $(\Omega_m, \Omega_\Lambda) = (1., 0.)$ (red) which are two sensible “extreme” cases. The dotted horizontal lines illustrate the upper limits on η for these cosmologies given the assumption $z_{s2} \leq 6.9$ (see §2.3).

The right panel of Fig. 6 shows $\eta(z_{s2})$ as a function of the second source redshift for two “extreme” flat cosmologies: $(\Omega_m, \Omega_\Lambda) = (0.3, 0.7)$ and $(\Omega_m, \Omega_\Lambda) = (1., 0.)$, intermediate cases lying in between. This shows that high values $\eta \gtrsim 1.57$ are not consistent with currently favored cosmologies. The upper limit on $\eta(z_{s2} = 6.9)$ is also shown for these two cases. This illustrates that very loose constraints can be obtained on cosmological parameters even if z_{s2} were known spectroscopically. Likewise, even assuming an isothermal slope of the density profile as motivated by joint lensing and dynamical analyses (Koopmans et al. 2006) does not drastically improve the constraints on η and consequently on cosmology as shown in Fig 7, even if z_{s2} could be measured with spectroscopic precision.

However, it is important to point out that the formal $\sim 3\%$ relative uncertainty we get on η from our lens

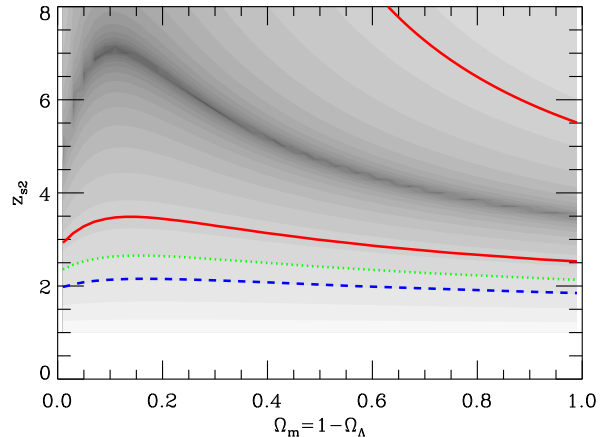


FIG. 7.— 68.3%, 95.4% and 99.3% CL contours in the redshift of source 2 and Ω_m parameter space assuming an isothermal density profile. This shows that even using strong priors on the density profile and for a given source redshift, only loose constraints can be inferred on cosmological parameters with a single double source plane system.

modeling strategy based on the identification of conjugate knots underestimates the potential accuracy of the method. Statistical errors would decrease by a factor of a few with a full modeling of the surface brightness distribution in the image plane. Unfortunately, the error budget would then be limited by additional systematic sources of uncertainty like extra convergence coming from large scale structures along the line of sight with estimated standard deviation $\sigma_\kappa \gtrsim 0.02$ (Dalal et al. 2005) or due to a non trivial environment in the main lens plane. Therefore, we conclude that it is unlikely that any cosmographic test based on the unique multiple Einstein ring system SDSSJ0946+1006 will provide valuable information on cosmological parameters. The prospects of using large numbers of double source plane lenses are investigated in §5.3.

5.2. Source 1, alias Lens 2

Among the massive perturbers along the line of sight to source 2, the most prominent is probably the mass associated with source 1. Since the lens modeling predicts that both sources are located very close to the optical axis (the center of the lens, see lower panels of Fig. 3), the light rays coming from source 2 to the observer will experience the potential of source 1 before that of the main lens. Fig. 8 illustrates the complexity of the configuration which adds some extra positive focusing for the second source plane. For the cosmological applications we mentioned above, this translates into a small but systematic source of bias. The bias introduced on the inferred mass profile of the main lens is small, so that the conclusions presented in §4 are not significantly altered except for the estimate of z_{s2} .

On the bright side, this lens configuration allows us to obtain some insight on the mass associated with Ring 1 (also identified as “Lens 2”) provided we now fully take into account the multiple lens plane nature of such lines of sight (e.g. Blandford & Narayan 1986; Schneider et al. 1992; Bartelmann 2003). This is the purpose of the present section, in which we fix the Λ CDM concordance cosmological model for simplicity.

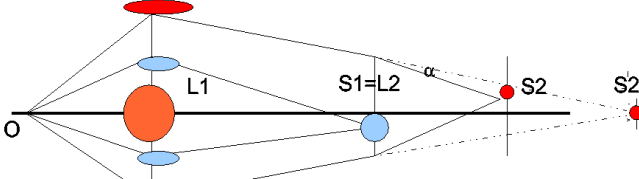


FIG. 8.— Sketch of the lensing optical bench with source 1 acting as a perturbing lens on source 2 which complicates the relation between redshifts, deflection angles and angular distances.

To achieve this goal we have to address the mass properties of the main lens at the same time as those of the first source 1. We reconsider the lens model of §3, but add another mass component at redshift $z_{l2} = z_{s1} = 0.609$ in the form of a singular isothermal sphere with free equivalent velocity dispersion parameter $\sigma_{\text{SIE},s1}$ and centered on the position of source 1. As in §3, our uncertainty on the distance to source 2 is simply parameterized by its redshift z_{s2} in the context of a Λ CDM cosmological model.

In multiple lens-plane theory, the relation between the angular position $\vec{\theta}_j$ of a light ray in the j -th lens plane and the angular position in the $j = 1$ image plane is:

$$\vec{\theta}_j(\vec{\theta}_1) = \vec{\theta}_1 - \sum_{i=1}^{j-1} \frac{D_{ij}}{D_j} \vec{\alpha}(\vec{\theta}_i). \quad (4)$$

The last lens plane N can be identified with the source plane such that $\vec{\theta}_N = \vec{\beta}$. In Eq. 4, as compared to Bartelmann (2003), we did not consider the *reduced* deflection which introduces an unnecessary extra D_{is}/D_s term in the sum. Likewise, the sign convention for the deflection is different than Bartelmann (2003). Therefore for two distinct positions $\vec{\theta}_1$ and $\vec{\theta}_2$ coming from two distinct source plane positions $\vec{\beta}_1$ and $\vec{\beta}_2$ respectively, we can write:

$$\begin{aligned} \vec{\beta}_1 &= \vec{\theta}_1 - \frac{D_{l1}}{D_{s1}} \vec{\alpha}(\vec{\theta}_1) \\ \vec{\beta}_2 &= \vec{\theta}_2 - \frac{D_{l2}}{D_{s2}} \vec{\alpha}(\vec{\theta}_2) - \frac{D_{s1s2}}{D_{s2}} \vec{\alpha}_{s1} \left(\vec{\theta}_2 - \frac{D_{l1}}{D_{s1}} \vec{\alpha}(\vec{\theta}_2) - \vec{\beta}_1 \right) \end{aligned} \quad (5)$$

In these equations, $\hat{\alpha}$ is the deflection produced by the main lensing galaxy (lying in the plane that also defines the image plane) and $\hat{\alpha}_{s1}$ is the perturbing deflection produced by source 1 (lens 2) onto source 2. Note that parameters like the center of source 1 enter the modeling scheme both as source- and lens-plane parameters. This is clearly visible in the brackets for the argument of $\hat{\alpha}_{s1}$ that contains $\vec{\beta}_1$, the position of source 1 in the source plane.

The constraints obtained on the equivalent velocity dispersion parameter of the main lens σ_{SIE} and that of source 1 $\sigma_{\text{SIE},s1}$ are shown in the left panel of Fig. 9. We clearly see two kinds of solutions: one (family *i*) has a high lens velocity dispersion (and slope $\gamma' \sim 1.96$, nearly isothermal) and little mass in source 1, whereas the other family (*ii*) has a lower main lens velocity dispersion and more mass in source 1. We measure $(\sigma_{\text{SIE}}, \sigma_{\text{SIE},s1}) = (295^{+3.5}_{-5.0}, 56 \pm 30) \text{ km s}^{-1}$ for family *i* and $(\sigma_{\text{SIE}}, \sigma_{\text{SIE},s1}) = (247.3^{+8.5}_{-5.7}, 104^{+21}_{-26}) \text{ km s}^{-1}$ for family *ii*.

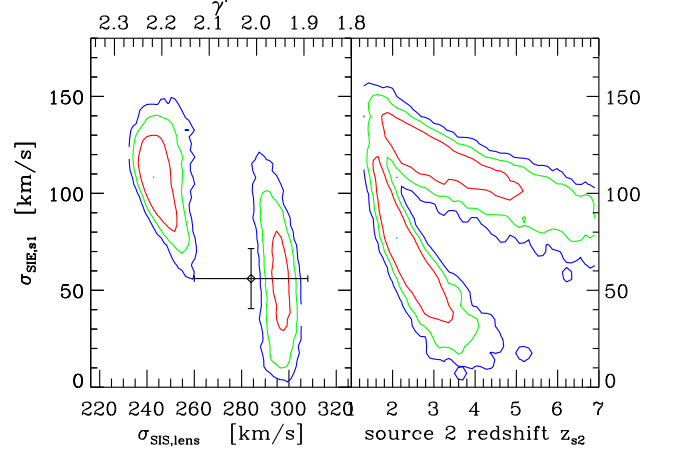


FIG. 9.— *Left panel:* contours in parameter space of the velocity dispersion of the main lens σ_{SIE} and that of the first source $\sigma_{\text{SIE},s1}$. Given the tight correlation $\sigma_{\text{SIE}} \simeq (687 - 200.3\gamma') \text{ km s}^{-1}$ found in §4, the upper abscissa shows the correspondence with slope γ' . The kinematical SDSS estimate of $\sigma_{v,*}$ and the velocity dispersion of source 1 inferred from the Tully-Fisher relation (Moran et al. 2007) are overlaid as a point with error bar. *Right panel:* contours in parameter space of the second source redshift z_{s2} and the velocity dispersion of the first source $\sigma_{\text{SIE},s1}$. The recovered z_{s2} strongly depends on the mass enclosed in source 1. In both panels confidence levels mark the 68.3, 95.4 and 99.3% enclosed probability.

A pixelised source plane inversion for both of these best fit models is shown in Fig. 10. Family *i* models are shown in the top row and family *ii* in the bottom row. Note the very complex systems of caustic and critical lines produced by this multiple lens plane system. It is difficult to favor either of these models based on a visual inspection and either region on the parameter space has about the same statistical weight (fraction of MCMC samples).

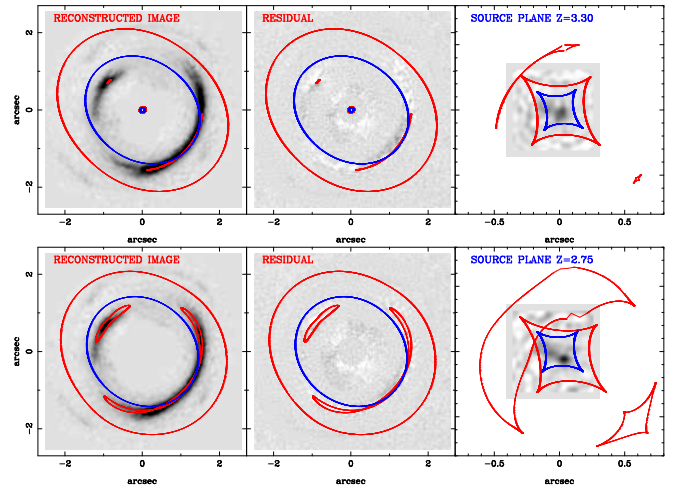


FIG. 10.— *Top panels:* Best fit family *i* model image and source plane reconstructions. From left to right reconstructed image plane, residual (data–model), and source 2 plane at redshift $z_{s2} = 3.30$. *Bottom panels:* idem for the best fit family *ii* models (with $z_{s2} = 2.75$). Note the complex critical and caustic curves for the z_{s2} source plane due to the multiple lens plane configuration produced by source 1. For both models the reconstruction is satisfying and produces very few residuals.

The left panel of Fig. 9 also shows the aperture-corrected SDSS-inferred velocity dispersion of the lens $\sigma_{v,*} = 284 \pm 24 \text{ km s}^{-1}$ which seems to favor family *i* solutions, based on the earlier SLACS results of a general agreement between stellar velocity dispersion and σ_{SIE} . In addition, we can get further external information on the mass of source 1, by extrapolating the Tully-Fisher relation found by Moran et al. (2007) at $z \sim 0.5$ for late-type galaxies. In the field, they found that at absolute magnitudes of $V \sim -19.7$, the maximum rotation velocity is $\log(2V_{\text{max}}) = 2.2 \pm 0.1$. Assuming $V_{\text{max}} \simeq \sqrt{2}\sigma_{\text{SIE}}$, this translates into an estimate $\sigma_{\text{SIE},s1} \simeq 59 \pm 13 \text{ km s}^{-1}$. Another piece of information comes from weak lensing results at intermediate redshift ($0.2 < z < 0.4$) by Hoekstra et al. (2005), who found that galaxies with magnitude $V - 5 \log h \simeq -19$ have virial masses $M_{\text{vir}} \simeq 1.50^{+0.99}_{-0.64} \times 10^{11} h_{70}^{-1} M_{\odot}$ which also corresponds to $\log(2V_{\text{max}}) = 2.20 \pm 0.09$, in good agreement with Moran et al. (2007). These two arguments also seem to favor family *i* solutions, i.e. those with more mass in the main lens and less in source 1.

The right panel of Fig. 9 shows the important degeneracy between the redshift of source 2 and the velocity dispersion of source 1. We can see that the more massive source 1, the lower z_{s2} must be. This demonstrates that any cosmographic test based on multiple source plane lens systems should carefully consider the mass in the foreground source as a significant perturbation on light rays coming from the most distant source. Adding a substantial amount of mass in source 1 significantly changes the inferred redshift of source 2 either for family *i* models which yields $z_{s2} = 2.6^{+1.0}_{-0.7}$ or family *ii* models yielding $z_{s2} = 3.8^{+1.9}_{-1.5}$. Marginalizing over the whole posterior PDF gives $z_{s2} = 3.1^{+2.0}_{-1.0}$.

TABLE 3
BEST-FIT MODEL PARAMETERS FOR SDSSJ0946+1006 USING A COMPOUND DOUBLE LENS PLANE.

| Parameter | family <i>i</i> | family <i>ii</i> | global |
|------------------------------------------|---------------------------|---------------------------|---------------------------|
| b_{∞} [arcsec] | $2.65^{+0.07}_{-0.10}$ | $1.91^{+0.07}_{-0.06}$ | $1.98^{+0.69}_{-0.11}$ |
| γ' | $1.96^{+0.03}_{-0.02}$ | $2.23^{+0.03}_{-0.05}$ | $2.18^{+0.07}_{-0.22}$ |
| axis ratio q | $0.889^{+0.057}_{-0.016}$ | $0.816^{+0.129}_{-0.027}$ | $0.879^{+0.067}_{-0.083}$ |
| PA_0 | $-15.9^{+9.5}_{-12.2}$ | $-17.9^{+9.2}_{-17.3}$ | $-17.0^{+9.3}_{-15.5}$ |
| γ_{ext} | $0.069^{+0.016}_{-0.009}$ | $0.089^{+0.026}_{-0.012}$ | $0.082^{+0.026}_{-0.016}$ |
| PA_{ext} | $-27.6^{+6.1}_{-6.7}$ | $-26.5^{+6.2}_{-6.7}$ | $-27.0^{+6.2}_{-6.7}$ |
| z_{s2} | $2.6^{+1.0}_{-0.7}$ | $3.8^{+1.9}_{-1.5}$ | $3.1^{+2.0}_{-1.0}$ |
| $\sigma_{\text{SIE},s1}$ [km s $^{-1}$] | $56.6^{+30.3}_{-27.6}$ | $108.9^{+18.0}_{-19.9}$ | $94.0^{+26.7}_{-46.6}$ |
| σ_{SIE} [km s $^{-1}$] | 295^{+3}_{-4} | 246^{+7}_{-5} | 254^{+43}_{-11} |

Best fit model parameters and 68.4% confidence limits. Angles are in degrees oriented from North to East.

5.3. Future outlook: cosmography with many double source plane lenses

In §5.1 we explored the possibility of constraining cosmology with SDSSJ0946+1006, and came to the conclusion that the errors are too large for this to be interesting. In §5.2 we saw that the mass of the closest source must be taken into account as a perturbation along the double source plane optical bench. Here we attempt to address the possibility of using large numbers of such

multiple lensing systems to probe the cosmology. Future space-based missions like DUNE or JDEM should provide us with tens of thousands of lenses, among which several tens would be double source plane systems. We also assume that redshifts will be available, from space- or ground-based spectroscopic follow-up.

First, we summarize the error budget expected for a typical double source plane system. As described before, the main quantity of interest is the ratio of distance ratios parameter $\eta \equiv (D_{\text{ls}}/D_{\text{os}})_2 / (D_{\text{ls}}/D_{\text{os}})_1$, where source 2 is the furthest one. For simplicity, we assume that the main lens, the first source, and the second source are perfectly aligned onto the optical axis, resulting in two complete concentric rings of radius θ_1 and θ_2 . The lens equation for each source plane reads:

$$\beta_1 = \theta_1 - (D_{\text{ls}}/D_{\text{os}})_1 \alpha_{\text{tot}}(\theta_1) = 0, \quad (7a)$$

$$\beta_2 = \theta_2 - (D_{\text{ls}}/D_{\text{os}})_2 \alpha_{\text{tot}}(\theta_2) = 0. \quad (7b)$$

We consider again the general power-law surface mass distribution of Eq. (1) producing deflections α_1 and α_2 on source 1 and source 2 light rays. For source 2 we must add α_p the *small* perturbing deflection¹¹ due to source 1 and experienced by source 2 only. Combining Eq. (7a) and Eq. (7b) gives:

$$\eta = \left(\frac{\theta_2}{\theta_1}\right)^{\gamma'-1} \frac{1}{1 + \frac{D_{s1s2}}{D_{ls2}} \frac{\alpha_p}{\alpha_2}}. \quad (8)$$

This equation shows the importance of the perturbation. If one aims at constraining η with interesting accuracy (i.e. error smaller than 0.01), the small perturbing term in the denominator of second part on the right hand side of Eq. (8) should be smaller than 0.01. Keeping in mind that for lensing potentials close to isothermal, $\alpha \propto \sigma^2$, and that the typical velocity dispersion of the main lens is about $\sigma \simeq 250 \text{ km s}^{-1}$, it is important to control and correct perturbing potentials with velocity dispersion as small as $\sigma_p = \sigma/10 \sim 30 \text{ km s}^{-1}$ for values $D_{s1s2}/D_{ls2} \simeq 0.5$.

Next, differentiating Eq. (8), and writing $r \equiv \theta_2/\theta_1$, one can infer the fractional error on η :

$$\left(\frac{\delta\eta}{\eta}\right)^2 = (\gamma' - 1)^2 \left(\frac{\delta r}{r}\right)^2 + (\ln r)^2 \delta\gamma'^2 + \frac{4}{\left(1 + \frac{D_{ls2}}{D_{s1s2}} \frac{\sigma_p^2}{\sigma^2}\right)^2} \left(\frac{\delta\sigma_p}{\sigma_p}\right)^2. \quad (9)$$

The first contribution is the relative measurement error on the ratio of Einstein radii, with typical values $0.001 \leq \delta r/r \leq 0.03$ for deep space based imaging. The second term captures our prior uncertainty on the slope of the density profile (for example Koopmans et al. (2006) measured $\langle\gamma'\rangle \simeq 2.01$ and an intrinsic scatter $\delta\gamma' \simeq 0.12$). Finally, the third term represents our prior knowledge of the mass of the perturber, which can be based, for example, on the Tully-Fisher relation. Moran et al. (2007)

¹¹ We assume that the non-linear coupling between lens planes can be neglected, i.e. the perturbation of source 1 is small compared to the deflection from the main lens on source 2 light rays: $\alpha_p \ll \alpha_2 \simeq \theta_2$.

estimated $\delta\sigma_p/\sigma_p \simeq 0.25$. Inserting those values into (9), and assuming a typical value of $r \simeq 1.5$, we find a relative uncertainty on $\delta\eta/\eta \simeq 0.06$ for a single system. The error is dominated by model uncertainties on the slope of the density profile and the mass in source 1. In the case of SDSSJ0946+1006, we achieve a similar accuracy when using the above priors on the slope and the velocity dispersion of source 1. In the following we shall use a conservative $\delta\eta/\eta = 0.08$ fiducial value.

Having estimated the accuracy achievable on η for a single double source plane system, we focus on the cosmological meaning of η in a spatially flat universe dominated by Dark Matter (Ω_m), and Dark Energy ($\Omega_{DE} = 1 - \Omega_m$) with equation of state parameter $w = p_{DE}/\rho_{DE}$. It is worth pointing out that the ratio of angular diameter distances is independent of the Hubble constant H_0 .

The constraints on (Ω_m, w) are shown in the right panel of Fig. 11. The error contours are obtained using a Fisher matrix formalism. We assumed a sample of 50 double source plane lenses, randomly produced using Monte-Carlo simulations. The redshift distribution of lenses and sources used for the Monte-Carlo simulations is shown in the upper left panel of Fig. 11. For the parent population of sources, it is based on recent COSMOS estimates (Leauthaud et al. 2007). The equivalent velocity dispersion of the lenses is assumed to be Gaussian with mean and standard deviation of 190 and 60 km s^{-1} respectively. The Einstein radii for the first and second ring are constrained to be greater than $0.7''$ and $1.0''$ respectively.

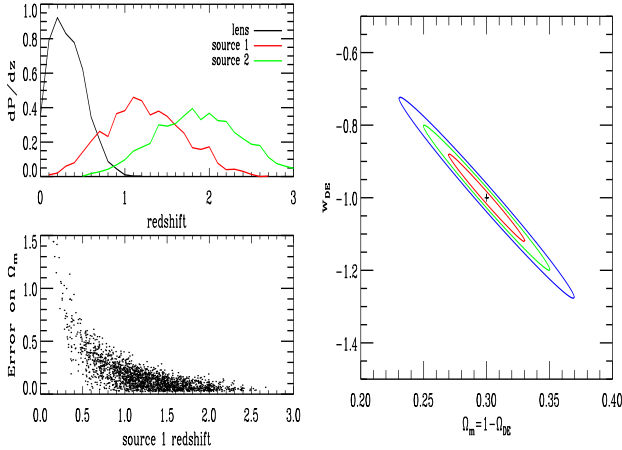


FIG. 11.— *Top left panel:* Redshift distribution for the lens, source 1 and source 2 used in the Monte-Carlo simulation of mock double source plane lenses as they could be discovered in future space-based surveys. *Bottom left panel:* Individual error brought by each system on Ω_m as a function of the redshift of the first source. *Right panel:* 68.3, 95.4 and 99.3% confidence levels contours on the matter density Ω_m and equation of state of dark energy $w = p/\rho$ obtained when combining 50 multiple source plane systems.

The cosmological parameters Ω_m and w are recovered with a precision ± 0.020 and ± 0.080 respectively. We note that the sensitivity and the orientation of the degeneracy in this set of cosmological parameters is similar to those obtained with a type Ia supernovae experiment (see *e.g.* Réfrégier et al. 2006, and references therein). The lower left panel of this figure demonstrates that the

systems that contribute the most to constraining Ω_m are those with source 1 redshift $z_{s1} \gtrsim 1$ (a similar trend is seen for w). Lens redshifts larger than ~ 0.5 are also more efficient configurations. This can easily be understood since the higher the redshifts of either lens, first or second source the more sensitive distances are on cosmological parameters. Note that situations with very low redshift lenses but high redshift source 1 and 2 will result in a rapid saturation of the D_{ls}/D_{os} for both source 1 and 2, leading to values $\eta \simeq 1$ independent on cosmology. The sensitivity on cosmology is actually essentially driven by the redshift of the primary lens. Therefore we conclude that SDSSJ0946+1006 is not an optimal double source plane lens system for cosmographic purposes.

However the prospects of doing cosmography with future samples of double source plane lenses are excellent, provided systematic effects are controlled. The main source of systematic uncertainty that was ignored in the above calculations is the possibility of a change in the mean density slope as a function of lens redshift $\langle\gamma'\rangle = f(z_l)$ as present data seem to suggest that the dynamical properties of early-type galaxies have not changed much since $z \sim 1$. Koopmans et al. (2006) found $d\langle\gamma'\rangle/dz = 0.23 \pm 0.16$ over the redshift range $[0.08, 1.01]$. Progress needs to be made along this line to improve our knowledge of $\langle\gamma'\rangle = f(z_l)$, but a great advantage of double source plane systems over single ones is that combining stellar dynamics and lensing constraints from two source planes would be more efficient at “self-calibrating” the method than using single ones. In addition a thorough lensing analysis aiming at carefully modeling the surface brightness of lensed structures will certainly help in controlling any such evolution trend of the density profile (see *e.g.* Dye & Warren 2007).

6. SUMMARY & CONCLUSION

In this paper we report the discovery of the first galaxy-scale double lensing event made of a foreground lens galaxy at redshift $z_l = 0.222$, a first source at redshift $z_{s1} = 0.609$ (Ring 1) and a more distant source (Ring 2) with unknown redshift, despite an attempt to measure its redshift with deep optical spectroscopy using LRIS on the Keck I Telescope. The detection of Ring 2 in a single orbit HST-ACS F814W filter image, sets an upper limit to its redshift $z_{s2} < 6.9$.

Modeling the geometry of the lensed features at different source planes we determine the mass density profile of the lens galaxy which is found to be close to isothermal. The best fit lens model predicts a stellar velocity dispersion in very good agreement with that measured from SDSS spectroscopy. The model requires a relatively large amount of dark matter inside the effective radius $f_{DM,2D}(< R_{eff}) \simeq 73 \pm 9\%$ (corresponding to a projected total mass-to-light ratio $M/L_V = 11.54 \pm 0.13 h_{70} (M/L_V)_\odot$), assuming the stellar mass to light ratio measured in paper IV. Along with the complex isophotes of the lens galaxy and the presence of several other (less luminous) galaxies at similar photometric redshifts, the high dark matter fraction suggests that the lens may be the central galaxy of a group scale halo. The high precision of this measurement – far superior to that attainable from a single multiply imaged systems – demonstrates that double source plane lenses are extremely valuable tools to study the mass profile of

galaxies and groups.

In order to constrain the redshift of Ring 2 and assess the feasibility of determining cosmological parameters using double source plane lenses, we constructed multiple lens plane mass models. In that case the lensing effect of Ring 1 on Ring 2 is taken into account and modeled as a singular isothermal sphere. Although the extra mass component adds additional uncertainty to the derived z_{s2} and cosmological parameters, it provides a unique way to determine the total mass of the intermediate galaxy (the inner Ring). Discarding the family *ii* range of solutions (disfavored by kinematics of stars on the main lens galaxy), the two-lens-plane mass model results can be summarized as follows:

- The redshift of Ring 2 is found to be $z_{s2} = 2.6^{+1.0}_{-0.7}$. This is a genuine prediction that can be tested with the help of deep Hubble images at shorter wavelengths, using the dropout technique.
- No interesting constraints on cosmological parameters can be obtained from the lensing analysis of the system SDSSJ0946+1006, due to the unknown redshift of Ring 2, the overall degeneracy of cosmography with the slope of the mass density profile between the rings, the degeneracy with the mass of the inner ring, and the suboptimal combination of lens and source redshifts.
- The velocity dispersion of Ring 1 is found to be $\sigma_{SIE} = 56 \pm 30 \text{ km s}^{-1}$, in good agreement with the value expected based on the extrapolation of Tully-Fisher relation at this redshift (Moran et al. 2007) and on weak-lensing measurements (Hoekstra et al. 2005). Given that lensing cross section increases with the fourth power of the velocity dispersion, individual lenses in this mass range are expected to be very rare. In addition, it is observationally more difficult to identify lensed background structures embedded in foreground late-type galaxies with small Einstein radius (both for imaging or spectroscopic lens searches). Thus by exploiting the boost of the primary lens, double source plane, also seen as double lens plane systems, may be an effective way to determine the lensing mass of small distant galaxies, complementing detailed photometric studies (Marshall et al. 2007), and kinematic studies with integral field spectrographs on large ground based telescopes with adaptive optics.

Future planned space missions like JDEM or DUNE are expected to deliver several tens of thousands of single source plane lenses (Aldering & the SNAP collaboration 2004; Marshall et al. 2005; Réfrégier et al. 2006) and several tens of double source plane lens galaxies. Given the great utility of multiple source plane lenses as tools to study distant galaxies, and the relatively small number of expected systems, we argue that the necessary effort of spectroscopic follow-up would be easily affordable and well motivated.

In addition, a relatively large sample of double source plane galaxy-scale gravitational lenses will be a practical

tool for cosmography. As an example, we calculated the constraints on Ω_m and the equation of state of Dark Energy $w = p_{DE}/\rho_{DE}$ that can be obtained from a sample of 50 double source plane lenses, assuming both source redshifts are known and are realistically distributed. Spectroscopic follow-up of such systems rings is also required to control systematic effects such as the change in the mean density profile slope as a function of the lens galaxy redshift. A careful analysis taking into account the uncertainty on the mass profile of the main lens and of the perturber shows that cosmological parameters can be measured with an accuracy of 10% comparable to that obtained from the Hubble diagram of Type Ia supernovae.

This research is supported by NASA through Hubble Space Telescope programs SNAP-10174, GO-10494, SNAP-10587, GO-10798, GO-10886. TT acknowledges support from the NSF through CAREER award NSF-0642621, the Sloan Foundation through a Sloan Research Fellowship. He is also supported by a Packard fellowship. The work of LAM was carried out at Jet Propulsion Laboratory, California Institute of Technology under a contract with NASA. L.V.E.K. is supported in part through an NWO-VIDI program subsidy (project number 639.042.505). He also acknowledges the continuing support by the European Community's Sixth Framework Marie Curie Research Training Network Programme, Contract No. MRTN-CT-2004-505183 "ANGLES". PJM acknowledges support from the Tabasco foundation in the form of a research fellowship. PJM is also grateful to Daniel Holz for useful early discussions on double lenses and their likely frequency. Based on observations made with the NASA/ESA Hubble Space Telescope, obtained at the Space Telescope Science Institute, which is operated by the Association of Universities for Research in Astronomy, Inc., under NASA contract NAS 5-26555. This project would not have been feasible without the extensive and accurate database provided by the Digital Sloan Sky Survey (SDSS). Funding for the creation and distribution of the SDSS Archive has been provided by the Alfred P. Sloan Foundation, the Participating Institutions, the National Aeronautics and Space Administration, the National Science Foundation, the U.S. Department of Energy, the Japanese Monbukagakusho, and the Max Planck Society. The SDSS Web site is <http://www.sdss.org/>. The SDSS is managed by the Astrophysical Research Consortium (ARC) for the Participating Institutions. The Participating Institutions are The University of Chicago, Fermilab, the Institute for Advanced Study, the Japan Participation Group, The Johns Hopkins University, the Korean Scientist Group, Los Alamos National Laboratory, the Max-Planck-Institute for Astronomy (MPIA), the Max-Planck-Institute for Astrophysics (MPA), New Mexico State University, University of Pittsburgh, University of Portsmouth, Princeton University, the United States Naval Observatory, and the University of Washington.

APPENDIX

DERIVATION OF THE PROBABILITY OF MULTIPLE LENSING

In this Appendix we estimate the probability of finding a double lens in a sample of lenses like SLACS. The first ingredient is the surface density on the sky of potential lens galaxies, given by:

$$N_{\text{gal}} = \int d\sigma \int dz_l \frac{dn_l}{d\sigma} p(z_l) \frac{dV}{dz_l}, \quad (\text{A1})$$

with $\frac{dV}{dz_l}$ the comoving volume per unit solid angle and redshift, and $\frac{dn_l}{d\sigma}$ the velocity dispersion function. For simplicity, we assume here that the shape of the velocity dispersion function does not evolve with redshift, but only in normalization as described by the $p(z_l)$ function. In practice, we consider the velocity dispersion function $\frac{dn}{d\sigma}$ measured by Sheth et al. (2003) at $z \sim 0.1$, which is of the form:

$$\frac{dn_l}{d\sigma} = \phi_* \left(\frac{\sigma}{\sigma_*} \right)^\alpha \frac{\beta}{\sigma \Gamma[\alpha/\beta]} \exp[-(\sigma/\sigma_*)^\beta]. \quad (\text{A2})$$

with $\phi_* = 0.0020 \pm 0.0001 \text{ h}_{70}^3 \text{ Mpc}^{-3}$, $\sigma_* = 88.8 \pm 17.7 \text{ km s}^{-1}$, $\alpha = 6.5 \pm 1.0$ and $\beta = 1.93 \pm 0.22$.

The number density of foreground galaxies producing a single strong lensing event on a source population s1 can be written as:

$$N_{s1} = \int dz_{s1} \int d\sigma \int dz_l \frac{dV}{dz_l} \frac{dn_l}{d\sigma} p(z_l) \frac{dN_{s1}}{dz_{s1}} X(\sigma, z_l, z_{s1}), \quad (\text{A3})$$

following Marshall et al. (2005). In this equation, $X(\sigma, z_l, z_{s1})$ is the cross-section for lensing. In most cases of scale-free gravitational lenses $X(\sigma, z_l, z_{s1})$ can be separated such that $X(\sigma, z_l, z_{s1}) = \sigma^{2\nu} g(z_l, z_{s1})$, σ^ν giving the overall strength of the lens. For the particular case of a singular isothermal sphere that we shall consider, $\nu = 2$ and $g \propto (D_{ls1}/D_{os1})^2 \Theta(z_{s1} - z_l)$, with $\Theta(x)$ the Heaviside step function.

If the lensing cross-section for a second population of sources s2 does not depend on the presence or properties of an already lensed population s1 galaxy, we can write:

$$N_{s1, s2} = \int dz_{s2} \int dz_{s1} \int d\sigma \int dz_l \frac{dV}{dz_l} \frac{dn_l}{d\sigma} p(z_l) \frac{dN_{s1}}{dz_{s1}} \frac{dN_{s2}}{dz_{s2}} X_1(\sigma, z_l, z_{s1}) X_2(\sigma, z_l, z_{s2}). \quad (\text{A4})$$

Combining Eq. (A1), (A3), (A4) and taking advantage of the separability of the dependency on σ and on redshifts, the ratio of the probability that a galaxy lenses a source at z_{s2} given that it is already lensing a source at z_{s1} over the probability for a galaxy to lens a source at z_{s2} is given by:

$$\frac{P(\text{lens s2} | \text{lens s1})}{P(\text{lens s2})} = \frac{P(\text{lens s2, lens s1})}{P(\text{lens s2}) P(\text{lens s1})} = \frac{N_{s1, s2} N_{\text{gal}}}{N_{s2} N_{s1}} \quad (\text{A5})$$

$$= \frac{\left[\int d\sigma \frac{dn_l}{d\sigma} \right] \times \left[\int d\sigma \frac{dn_l}{d\sigma} \sigma^8 \right] \left[\int dV(z_l) p(z_l) \right] \times \left[\int dz_{s1} \frac{dN_{s1}}{dz_{s1}} \int dz_{s2} \frac{dN_{s2}}{dz_{s2}} \int dV(z_l) p(z_l) g(z_l, z_{s1}) g(z_l, z_{s2}) \right]}{\left[\int d\sigma \frac{dn_l}{d\sigma} \sigma^4 \right]^2 \left[\int dz_{s1} \frac{dN_{s1}}{dz_{s1}} \int dV(z_l) p(z_l) g(z_l, z_{s1}) \right] \times \left[\int dz_{s2} \frac{dN_{s2}}{dz_{s2}} \int dV(z_l) p(z_l) g(z_l, z_{s2}) \right]} \quad (\text{A6})$$

$$\equiv \Sigma \times \zeta. \quad (\text{A7})$$

where $dV(z_l)$ indicates $\frac{dV}{dz_l} dz_l$. The first term Σ in Eq. (A6) describes the strong dependency of the lensing cross section on velocity dispersion. As expected because lensing favors high σ systems, using the velocity dispersion function from Sheth et al. (2003), we estimate it to be larger than unity, of order $\Sigma = \Gamma((8+\alpha)/\beta) \Gamma(\alpha/\beta) / \Gamma((4+\alpha)/\beta)^2 \simeq 2.44$.

The second term ζ contains volume and lensing efficiency $g(z_l, z_s)$ effects that depend on the redshifts of the lens and the sources. By defining a lensing efficiency averaged over a given population of sources,

$$G_i(z_l) = \int dz_{si} \frac{dN_i}{dz_{si}} g(z_l, z_{si}), \quad (\text{A8})$$

we can simplify the second term in Eq. (A6) and write it as:

$$\zeta = \frac{\left[\int dV(z_l) p(z_l) \right] \times \left[\int dV(z_l) p(z_l) G_1(z_l) G_2(z_l) \right]}{\left[\int dV(z_l) p(z_l) G_1(z_l) \right] \times \left[\int dV(z_l) p(z_l) G_2(z_l) \right]}. \quad (\text{A9})$$

To obtain a quantitative estimate of the probability of double lensing, let us consider some specific examples. The most important quantity in the definition of ζ is the comoving redshift distribution of deflectors $p(z_l)$. If all of them were confined in a single lens plane such that $p(z_l) = \delta(z_l - z_{l0})$, then $\zeta = 1$ and most of the change in probability comes from selection effects captured by Σ . If, instead, deflectors are broadly distributed over a range of redshifts, the ratio can be significantly higher than one because the probability of single lensing would be low for high redshift deflectors whereas the fact that a deflector is already lensing a source at z_{s1} favors lenses in a low redshift range, more suitable for lensing a source at z_{s2} .

We illustrate this volume effect by assuming that the comoving density of deflectors is constant out to a redshift z_{max} and then it drops to zero, that is $p(z_l) = \Theta(z_{\text{max}} - z_l)$. We also assume the redshift distribution of background sources

is of the form $dN/dz \propto e^{-z/z_0} (z/z_0)^{a-1}$. Population s2 galaxies follow the redshift distribution of faint background sources presented in Gavazzi et al. (2007) and having $z_0 = 0.345$ and $a = 3.89$. We use a redshift distribution for the s1 population that peaks around redshift 0.5, in agreement with the properties of spectroscopically discovered SLACS lenses (see Bolton et al. 2008). This corresponds to $z_0 \simeq 0.07$ and $a \simeq 7$. Note that the detailed shape of the redshift distribution for either s1 or s2 galaxies does not change the trends significantly, so this approximation is sufficient for our purposes. Fig. A1 shows the evolution of ζ as a function of the limiting redshift z_{\max} . We see that, out to reasonable values $z_{\max} \simeq 0.5$, ζ does not depart much from unity.

To obtain a numerical value to be compared with our SLACS sample, we consider a population of deflectors constant out to redshift unity. The gain in probability is $P(\text{lens s2} | \text{lens s1}) / P(\text{lens s2}) \simeq 2.4 - 5$. In other words, if one elliptical galaxy at $z \lesssim 0.8$ is about 200 is strongly lensing a faint background source, a strong lens in approximately 40–80 is a double lens. This is consistent with the observations.

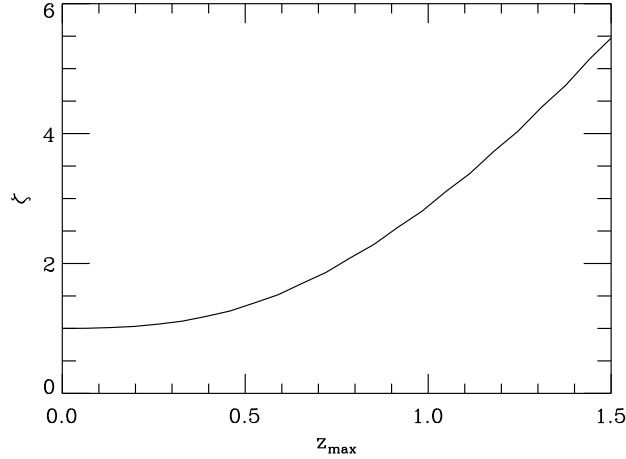


FIG. A1.— Evolution of the ζ term for multiple lensing probability boost $P(\text{lens s2} | \text{lens s1}) / P(\text{lens s2})$ as a function of the limiting redshift z_{\max} of the lens distribution.

REFERENCES

- Aldering, G. & the SNAP collaboration. 2004, astro-ph/0405232
 Barnabè, M. & Koopmans, L. V. E. 2007, ApJ, 666, 726
 Bartelmann, M. 2003, astro-ph/0304162
 Bell, E. F., Naab, T., McIntosh, D. H., et al. 2006, ApJ, 640, 241
 Blandford, R. & Narayan, R. 1986, ApJ, 310, 568
 Bolton, A. S., Burles, S., Koopmans, L. V. E., Treu, T., & Moustakas, L. A. 2005, ApJ, 624, L21
 Bolton, A. S., Burles, S., Koopmans, L. V. E., Treu, T., & Moustakas, L. A. 2006a, ApJ, 638, 703
 Bolton, A. S., Burles, S., Schlegel, D. J., Eisenstein, D. J., & Brinkmann, J. 2004, AJ, 127, 1860
 Bolton, A. S., Burles, S., Treu, T., Koopmans, L. V. E., & Moustakas, L. A. 2007, ApJ, 665, L105
 Bolton, A. S., Burles, S., Treu, T., et al. 2008, in preparation
 Bolton, A. S., Moustakas, L. A., Stern, D., et al. 2006b, ApJ, 646, L45
 Brainerd, T. G., Blandford, R. D., & Smail, I. 1996, ApJ, 466, 623
 Brewer, B. J. & Lewis, G. F. 2006, ApJ, 637, 608
 Cabanac, R. A., Alard, C., Dantel-Fort, M., et al. 2007, A&A, 461, 813
 Casertano, S., de Mello, D., Dickinson, M., et al. 2000, AJ, 120, 2747
 Conroy, C., Prada, F., Newman, J. A., et al. 2007, ApJ, 654, 153
 Dalal, N., Hennawi, J. F., & Bode, P. 2005, ApJ, 622, 99
 Dye, S., Smail, I., Swinbank, A. M., Ebeling, H., & Edge, A. C. 2007, MNRAS, 379, 308
 Dye, S. & Warren, S. 2007, astro-ph/0708.0787, 708
 Gavazzi, R., Fort, B., Mellier, Y., Pelló, R., & Dantel-Fort, M. 2003, A&A, 403, 11
 Gavazzi, R., Treu, T., Rhodes, J. D., et al. 2007, ApJ, 667, 176
 Gerhard, O., Kronawitter, A., Saglia, R. P., & Bender, R. 2001, AJ, 121, 1936
 Golse, G., Kneib, J.-P., & Soucail, G. 2002, A&A, 387, 788
 Hoekstra, H., Hsieh, B. C., Yee, H. K. C., Lin, H., & Gladders, M. D. 2005, ApJ, 635, 73
 Hoekstra, H., Yee, H. K. C., & Gladders, M. D. 2004, ApJ, 606, 67
 Kochanek, C. S., Falco, E. E., Impey, C. D., et al. 1999, in American Institute of Physics Conference Series, Vol. 470, After the Dark Ages: When Galaxies were Young (the Universe at $2 \leq z \leq 5$), ed. S. Holt & E. Smith, 163–
 Kochanek, C. S. & Narayan, R. 1992, ApJ, 401, 461
 Koopmans, L. V. E. 2005, MNRAS, 363, 1136
 Koopmans, L. V. E. 2006, in Engineering and Science, Vol. 20, EAS Publications Series, ed. G. A. Mamon, F. Combes, C. Deffayet, & B. Fort, 161–166
 Koopmans, L. V. E., Treu, T., Bolton, A. S., Burles, S., & Moustakas, L. A. 2006, ApJ, 649, 599
 Leauthaud, A., Massey, R., Kneib, J.-P., et al. 2007, ApJS, 172, 219
 Mandelbaum, R., Seljak, U., Kauffmann, G., Hirata, C. M., & Brinkmann, J. 2006, MNRAS, 368, 715
 Marshall, P., Blandford, R., & Sako, M. 2005, New Astronomy Review, 49, 387
 Marshall, P. J., Treu, T., Melbourne, J., et al. 2007, ApJ in press, astro-ph/0710.0637, 710
 Moran, S. M., Loh, B. L., Ellis, R. S., et al. 2007, ApJ, 665, 1067
 Moustakas, L. A., Marshall, P., Newman, J. A., et al. 2007, ApJ, 660, L31
 Myers, S. T., Jackson, N. J., Browne, I. W. A., et al. 2003, MNRAS, 341, 1
 Oyaizu, H., Lima, M., Cunha, C. E., et al. 2007, astro-ph/0708.0030, 708
 Peng, C. Y., Ho, L. C., Impey, C. D., & Rix, H. 2002, AJ, 124, 266
 Prada, F., Vitvitska, M., Klypin, A., et al. 2003, ApJ, 598, 260
 Ratnatunga, K. U., Griffiths, R. E., & Ostrander, E. J. 1999, AJ, 117, 2010

- Réfrégier, A., Boulade, O., Mellier, Y., et al. 2006, in Presented at the Society of Photo-Optical Instrumentation Engineers (SPIE) Conference, Vol. 6265, Space Telescopes and Instrumentation I: Optical, Infrared, and Millimeter. Edited by Mather, John C.; MacEwen, Howard A.; de Graauw, Mattheus W. M.. Proceedings of the SPIE, Volume 6265, pp. 62651Y (2006).
- Rubin, V. C., Peterson, C. J., & Ford, Jr., W. K. 1980, ApJ, 239, 50
- Schlegel, D. J., Finkbeiner, D. P., & Davis, M. 1998, ApJ, 500, 525
- Schneider, P., Ehlers, J., & Falco, E. E. 1992, Gravitational Lenses (Springer-Verlag Berlin Heidelberg New York)
- Sheldon, E. S., Johnston, D. E., Frieman, J. A., et al. 2004, AJ, 127, 2544
- Sheth, R. K., Bernardi, M., Schechter, P. L., et al. 2003, ApJ, 594, 225
- Soucail, G., Kneib, J.-P., & Golse, G. 2004, A&A, 417, L33
- Suyu, S. H., Marshall, P. J., Hobson, M. P., & Blandford, R. D. 2006, MNRAS, 371, 983
- Swaters, R. A., Madore, B. F., van den Bosch, F. C., & Balcells, M. 2003, ApJ, 583, 732
- Treu, T., Koopmans, L. V., Bolton, A. S., Burles, S., & Moustakas, L. A. 2006, ApJ, 640, 662
- Treu, T. & Koopmans, L. V. E. 2002, ApJ, 575, 87
- Treu, T. & Koopmans, L. V. E. 2004, ApJ, 611, 739
- Trujillo, I., Burkert, A., & Bell, E. F. 2004, ApJ, 600, L39
- van Albada, T. S., Bahcall, J. N., Begeman, K., & Sancisi, R. 1985, ApJ, 295, 305
- Warren, S. J. & Dye, S. 2003, ApJ, 590, 673
- Warren, S. J., Hewett, P. C., Lewis, G. F., et al. 1996, MNRAS, 278, 139
- Wayth, R. B. & Webster, R. L. 2006, MNRAS, 372, 1187